Dynamics of Surface Catalyzed Reactions; the Roles of Surface Defects, Surface Diffusion, and Hot Electrons†

Gabor A. Somorjai,* Kaitlin M. Bratlie, Max O. Montano, and Jeong Y. Park

Department of Chemistry, University of California, Berkeley, California 94720, and Materials Sciences Division and Chemical Sciences Division, Lawrence Berkeley National Laboratory, Berkeley, California 94720

Received: April 26, 2006; In Final Form: June 9, 2006

The mechanism that controls bond breaking at transition metal surfaces has been studied with sum frequency generation (SFG), scanning tunneling microscopy (STM), and catalytic nanodiodes operating under the high-pressure conditions. The combination of these techniques permits us to understand the role of surface defects, surface diffusion, and hot electrons in dynamics of surface catalyzed reactions. Sum frequency generation vibrational spectroscopy and kinetic measurements were performed under 1.5 Torr of cyclohexene hydrogenation/dehydrogenation in the presence and absence of H_2 and over the temperature range 300−500 K on the Pt(100) and Pt(111) surfaces. The structure specificity of the Pt(100) and Pt(111) surfaces is exhibited by the surface species present during reaction. On Pt(100), π-allyl *c*-C_6H_9, cyclohexyl (C_6H_{11}), and 1,4-cyclohexadiene are identified adsorbates, while on the Pt(111) surface, π-allyl *c*-C_6H_9, 1,4-cyclohexadiene, and 1,3-cyclohexadiene are present. A scanning tunneling microscope that can be operated at high pressures and temperatures was used to study the Pt(111) surface during the catalytic hydrogenation/dehydrogenation of cyclohexene and its poisoning with CO. It was found that catalytically active surfaces were always disordered, while ordered surface were always catalytically deactivated. Only in the case of the CO poisoning at 350 K was a surface with a mobile adsorbed monolayer not catalytically active. From these results, a CO-dominated mobile overlayer that prevents reactant adsorption was proposed. By using the catalytic nanodiode, we detected the continuous flow of hot electron currents that is induced by the exothermic catalytic reaction. During the platinum-catalyzed oxidation of carbon monoxide, we monitored the flow of hot electrons over several hours using a metal−semiconductor Schottky diode composed of Pt and TiO_2. The thickness of the Pt film used as the catalyst was 5 nm, less than the electron mean free path, resulting in the ballistic transport of hot electrons through the metal. The electron flow was detected as a chemicurrent if the excess electron kinetic energy generated by the exothermic reaction was larger than the effective Schottky barrier formed at the metal−semiconductor interface. The measurement of continuous chemicurrent indicated that chemical energy of exothermic catalytic reaction was directly converted into hot electron flux in the catalytic nanodiode. We found the chemicurrent was well-correlated with the turnover rate of CO oxidation separately measured by gas chromatography.

I. Introduction

Professor Charles Harris has spent much of his distinguished carrier tracking the energy and time distribution of high-speed electrons excited at metal surfaces.[1] The dynamics reveal the presence of trapped states, which elucidate mechanisms of electron exit trapping and dynamics.

In search of the dynamics of surface catalytic reactions, my laboratory has spent nearly three decades determining what controls bond breaking, such as H−H, C−H, and C−C, at transition metal surfaces. We developed instruments in our laboratory capable of monitoring surface reaction in situ; shown in Figure 1. First, we started with low-energy electron diffraction (LEED) to develop the capabilities to determine the surface structure of clean metal surfaces and adsorbed molecules as shown in Figure 1a.[2] Then, an instrument called molecular beam surface scattering was developed,[3] which operated under ultra-high-vacuum conditions and determined which metal single-crystal surfaces would break bonds (H−H by H_2/D_2 exchange and C−H exchange like in methane). We then constructed high-pressure cells in the middle of ultrahigh-vacuum (UHV) chambers to carry out catalytic reactions on small surface areas ($\sim$1 cm^2) of platinum, rhodium, and iron at high pressures, allowing experimental conditions to be close to those used in chemical technology.[4] We monitored the rates of reactions and product distribution by gas chromatography or other sensitive techniques (ammonia formation by photoionization, for example). Still, we could prepare clean surfaces in UHV and characterize them in UHV before and after the high-pressure catalytic reactions without ever exposing the crystal surfaces to air.

We found that UHV experiments exhibit discontinuous behavior from the high-pressure regime, where the experimental condition is in equilibrium with reactant gas, to low-pressure conditions. We have developed instruments for high-pressure catalytic reactions because the high turnover of catalytic reactions requires high pressures. These techniques have enabled us to detect surface intermediates on single-crystal surfaces under reaction conditions, elucidating the molecular reaction

† Part of the special issue "Charles B. Harris Festschrift".

* To whom correspondence should be addressed. E-mail: somorjai@berkeley.edu.

10.1021/jp062569d CCC: $33.50
Published on Web 07/25/2006

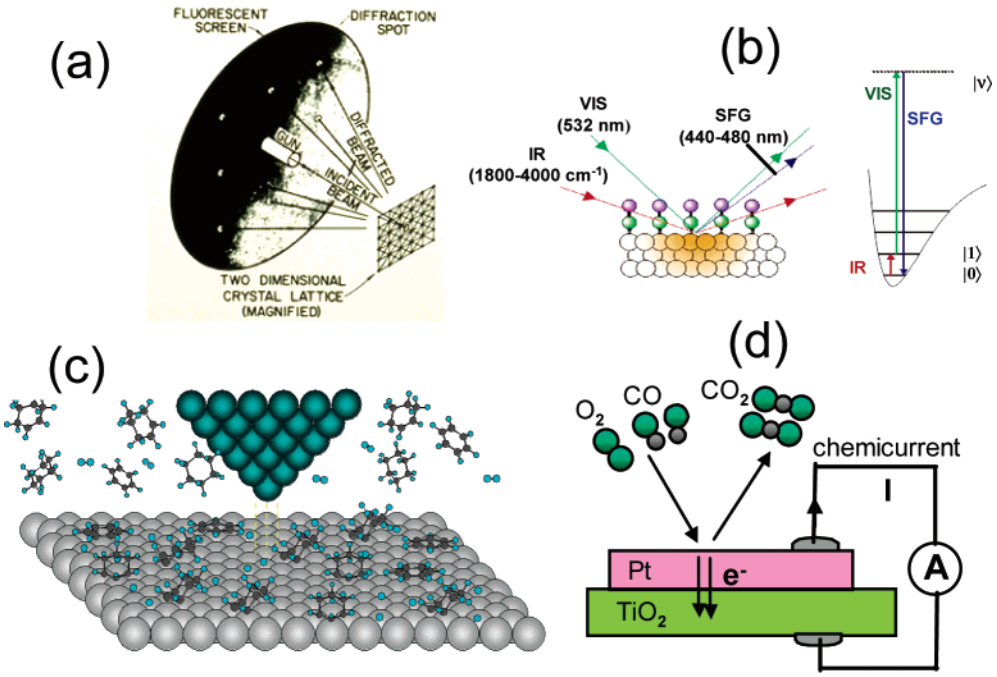

Figure 1. Schematics of (a) low-energy electron diffraction, (b) high-pressure sum frequency generation, (c) high-pressure scanning tunneling microscopy during cyclohexane hydrogenation/dehydrogenation process, and (d) Pt/TiO_2 catalytic nanodiode in CO oxidation.

mechanisms. Sum frequency generation vibrational spectroscopy, a two-photon laser spectroscopy,[5] is an extremely surface sensitive technique (as shown in Figure 1b), which allows for just that under reaction conditions. Finally, high-pressure scanning tunneling microscopy[6] was developed in our laboratory to permit monitoring of the mobile surface intermediates under reaction conditions and immobile surface species during poisoning. The scheme of high-pressure STM is illustrated in Figure 1c. A new molecular picture of the catalytic surface reaction dynamics emerges with the determination of chemical bond breaking on metal surfaces and the requirement of mobility of reactive surface species under catalytic conditions.

In this paper, we give examples of what has been learned from each instrument about surface reaction or surface catalytic reactions. At the end of the paper, we introduce the newest experimental development, the catalytic nanodiode,[7] which proves that during catalytic exothermic reaction conditions high kinetic energy, so-called "hot electrons", flow in the metal as illustrated in Figure 1d. If appropriately collected using a Schottky diode (a semiconductor catalytic metal junction like Pt/TiO_2 or Pt/GaN), a hot electron current can be detected that influences the chemistry of the semiconductor metal interface. This interesting effect has been in the literature for over five decades and has yet to be explored in detail.

II. SFG Studies of Cyclohexene Hydrogenation/Dehydrogenation on Platinum Single Crystals

Significant attention has been paid to cyclohexene chemistry on the single-crystal platinum surfaces, since it is considered prototypical of cyclic hydrocarbon conversion processes during naphtha reforming.[8] Not only is cyclohexene only one of the possible reaction intermediates when cyclohexane (C_6H_{10}) is dehydrogenated to benzene (C_6H_6), but it is also a reactant molecule in the hydrogenation to cyclohexane and dehydrogenation to benzene. Differences in turnover rates proves that the cyclohexene hydrogenation/dehydrogenation on platinum surfaces is a structure-sensitive reaction,[9] allowing cyclohexene to be a useful probe molecule.

Cyclohexene adsorption under UHV conditions has been extensively studied on the Pt(111) and Pt(100) surfaces using thermal desorption spectroscopy (TDS),[10−12] reflection adsorption infrared spectroscopy (RAIRS),[10] electron energy loss spectroscopy (EELS),[10] bismuth postdosing TDS (BPTDS),[12,13] laser-induced thermal desorption (LITD),[11] high-resolution electron energy loss spectroscopy (HREELS),[10,11] and SFG.[14−19] Briefly, cyclohexene exists in a di-σ form on the Pt(100) and Pt(111) surfaces at 100 K. Di-σ-cyclohexene is transformed to π-allyl c-C_6H_9 as the surface temperature is increased to 200 K. Dehydrogenation and benzene desorption results from further increasing the surface temperature.[10] Decomposition of benzene occurs at temperatures above 300 K.[11,13,20] Surface species present at low temperatures in UHV environments may not be the same as those species that are adsorbed under catalytically relevant conditions found at high pressures/temperatures or under an excess of hydrogen, thus necessitating the need to conduct these experiments under high-pressure environments.

II.A. Experimental Setup of Sum Frequency Generation. All experiments were carried out on a Pt single-crystal surface in a high-pressure/ultrahigh-vacuum (HP/UHV) system. The HP/UHV system is composed of a UHV chamber with a base pressure of 2×10^{-9} Torr and a HP cell isolated from the UHV chamber by a gate valve. The UHV chamber is equipped with an Auger electron spectrometer (AES), quadrupole mass spectrometer (QMS), and an Ar^+ sputter gun. The sample is transferred along a horizontal linear path between the UHV chamber and the HP cell using a magnetically coupled transfer arm. The 600-mL stainless steel HP cell has several ports and is electroplated with gold to reduce catalytic reactivity. A leak valve connects the gas line to the UHV chamber/QMS and can be used to sample the gas products during reaction. Two CaF_2 con flat windows on the HP cell are mounted 120° with respect to one another allowing transmission of infrared (IR), visible (vis), and sum frequency radiation during experiments. The HP cell is equipped with a recirculation loop that includes a diaphragm pump and inlet for gas chromatographic analysis. In GC analysis, a gaseous mobile phase flows under pressure

through a heated packed column. Once on the column, separation of a mixture occurs according to the relative lengths of time spent by its components in the stationary phase. The reactant and product gases were constantly mixed via a recirculation pump, while kinetics were determined via periodically sampling the reaction mixture and measuring mol % gas-phase composition using flame ionization detection and a packed column (0.1% AT-1000 on Graphpac GC 80/100 Alltech). The operating pressure in the HP cell is measured with two capacitance manometers, for pressure ranges between 0.1 and 1000 mTorr and between 0.1 and 1000 Torr.

A Nd:YAG laser (1064-nm fundamental having a 20-ps long pulse with a 20-Hz repetition rate) was used to perform the SFG experiments as illustrated in Figure 1b. The 1064-nm beam was frequency-doubled to 532 nm in a β-BaB_2O_4 (BBO) crystal. The tunable IR beam was generated in a $LiNbO_3$ by difference frequency mixing of the 1064 nm beam with the output of a $KTiOPO_4$ (KTP) optical parametric generator/amplifier (OPA/OPG) pumped by the 532-nm beam. The vis beam (200 μJ) and the IR (200 μJ) beams were spatially and temporally overlapped on the Pt(100) and Pt(111) surfaces with incident angles of 55° and 60°, respectively, with respect to the surface normal. All spectra were taken using a ppp polarization combination (SFG, vis, and IR beams were all p-polarized). The generated SFG beam was sent through a monochromator and the signal intensity was detected with a photomultiplier tube, and a gated integrator as the IR beam was scanned over the range of interest.

SFG technique and theory have been described in detail previously.[21−23] SFG is a second-order nonlinear optical process in which an infrared laser beam at ω_{IR} is combined with a visible laser beam at ω_{vis} to create a sum frequency output at $\omega_{SF} = \omega_{IR} + \omega_{vis}$, seen in Figure 1b. In SFG experiments, a visible and a tunable infrared beam are spatially and temporally overlapped on the surface. As the infrared beam is scanned over the frequency range of interest, vibrational spectra of the molecules present on the surface are obtained. SFG signals from molecules in the gas phase and the metal bulk are negligible, because $\chi^{(2)} = 0$ for centrosymmetric or isotropic media, under the electric dipole approximation. The center of inversion is broken at the interface, giving rise to a surface specific signal.

II.B. Results and Discussions. The discontinuity between UHV and high-pressure experiments is readily illustrated when Pt(111) is introduced to an environment of 1.5 Torr of cyclohexene (Figure 2). At 303 K, 1,4-cyclohexadiene (illustrated in Scheme 1b) is adsorbed on Pt(111). Increasing the surface temperature produces a surprising effect in that the 1,4-cyclohexadiene is hydrogenated to π-allyl c-C_6H_9 (shown in Scheme 1a); heating hydrocarbons on a platinum surface in the absence of H_2 usually leads to dehydrogenation and decomposition.[10,11,13,20] Further heating dehydrogenates the π-allyl c-C_6H_9 to 1,3-cyclohexadiene (see Scheme 1c).

1,4-Cyclohexadiene and 1,3-cyclohexadiene were found to coexist on Pt(111) at 303 K in the presence of excess hydrogen (15 Torr) and soon after hydrogenate to π-allyl c-C_6H_9 at 323 K, as see in Figure 3. π-Allyl c-C_6H_9 dehydrogenates to 1,3-cyclohexadiene when the surface temperature is increased to 400 K. Investigations in our laboratory of cyclohexene hydrogenation and dehydrogenation on the Pt(111) surface include kinetic measurements. Kinetic measurements, in conjunction with spectroscopic evidence, point toward π-allyl c-C_6H_9 hydrogenation being the rate-limiting step in cyclohexene hydrogenation, and 1,3-cyclohexadiene dehydrogenation is the rate-limiting step for benzene formation.[14] One possible reaction

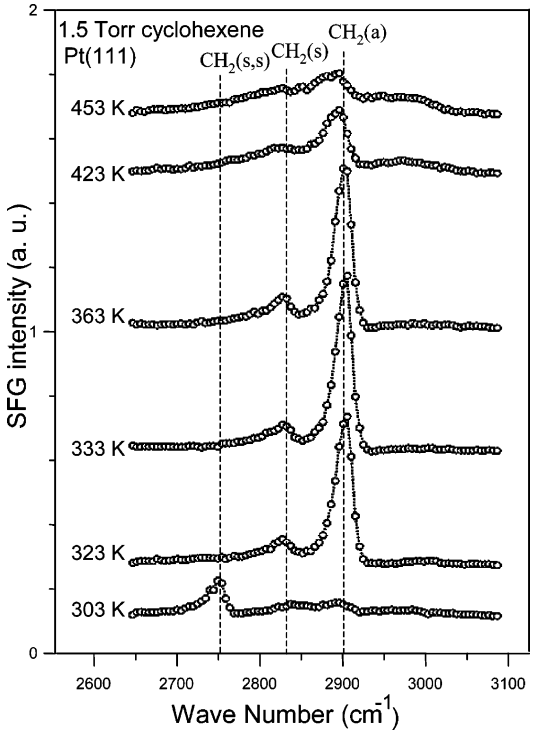

Figure 2. Temperature-dependent SFG spectra of surface species on Pt(111) under 1.5 Torr of cyclohexene in the range 303−483 K. Dotted lines are drawn for visual aids.

SCHEME 1: Schematic Diagram of (a) π-Allyl c-C_6H_9, (b) Quadra-σ-1,4-cyclohexadiene (C_6H_8), (c) 1,3-Cyclohexadiene (C_6H_8), and (d) Cyclohexyl (C_6H_{11}) Intermediates

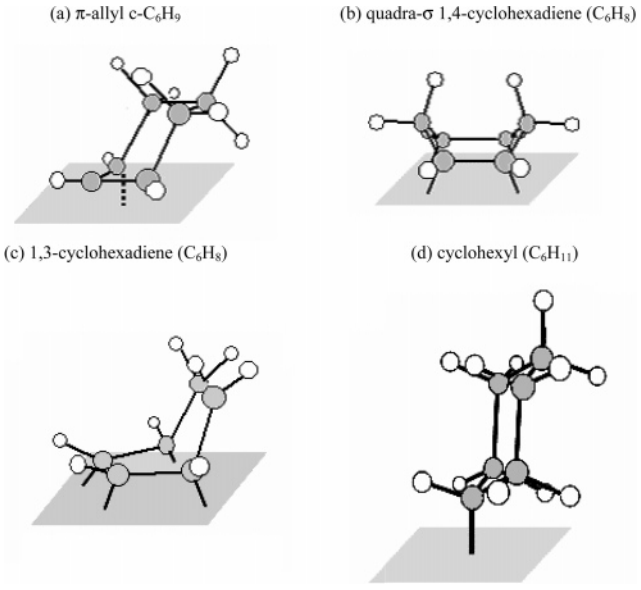

pathway for the formation of π-allyl c-C_6H_9 occurs via dehydrogenation of di-σ-C_6H_{10}. This reaction pathway allows

$$C_6H_{10} \rightarrow C_6H_9 + H \qquad \text{(R1)}$$

for a bimolecular reaction channel, allowing surface intermediates and the excess cyclohexene to react. We propose a bimolecular reaction between π-allyl c-C_6H_9 and the excess gas-phase cyclohexene. This newly generated cyclohexyl will further

$$C_6H_9 + C_6H_{10}\,(\text{excess}) \rightarrow C_6H_8 + C_6H_{11} \qquad \text{(R2)}$$

hydrogenate to form cyclohexane.

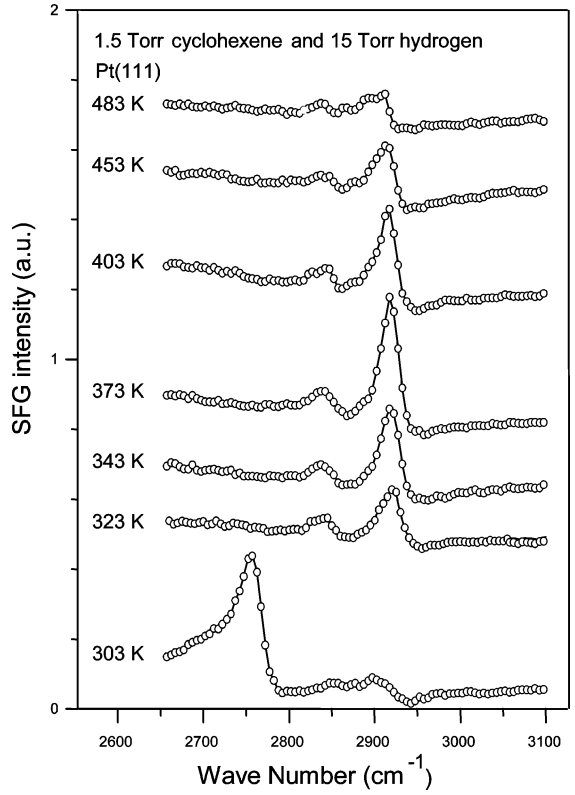

Figure 3. Temperature-dependent SFG spectra of surface species on Pt(111) under 1.5 Torr of cyclohexene and 15 Torr of H_2 in the range 303−453 K. Dotted lines are drawn for visual aids.

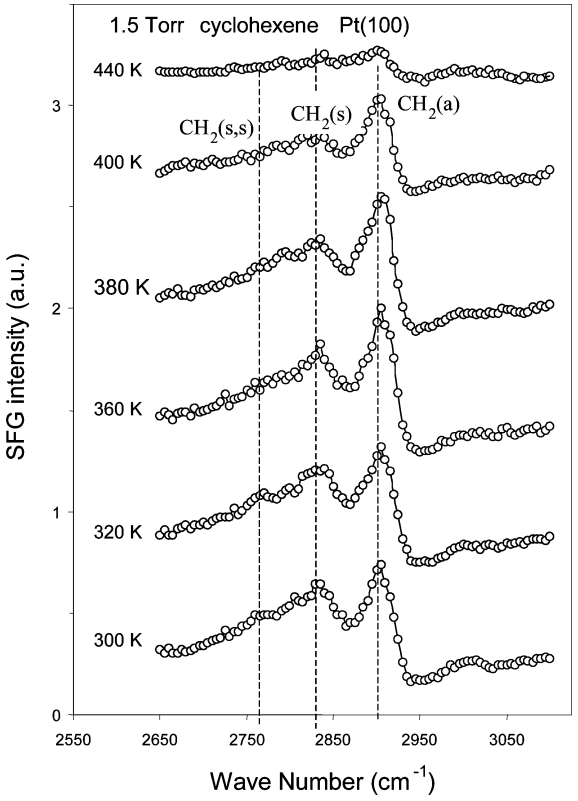

Figure 4. Temperature-dependent SFG spectra of surface species on Pt(100) under 1.5 Torr of cyclohexene in the range 300−440 K. Dotted lines were drawn for visual aids.

The kinetics and surface intermediates of cyclohexene hydrogenation and dehydrogenation have also been investigated on the Pt(100) surface under a range of temperatures (300−460 K) in the presence and absence of excess hydrogen (15 Torr). Three distinct surface intermediates have been identified through SFG measurements on the Pt(100) surface including π-allyl c-C_6H_9, 1,4-cyclohexadiene (C_6H_8), and cyclohexyl (C_6H_{11}) (shown in Scheme 1d).[20] Hydrogenated and dehydrogenated surface species have been detected in both the presence and absence of excess hydrogen as seen in Figures 4 and 5. Notable differences exist between the Pt(100) and Pt(111) surfaces as parameters such as the presence of excess hydrogen and surface temperature are altered. π-Allyl c-C_6H_9 and cyclohexyl have been found to coexist on the Pt(100)[24] surface until the pressure of cyclohexene is increased to 1.5 Torr, whereupon 1,4-cyclohexadiene becomes coadsorbed with π-allyl c-C_6H_9 and cyclohexyl as seen in Figure 2. The dominant surface species on the Pt(111) surface is π-allyl c-C_6H_9 until the cyclohexene pressure is increased to 1.5 Torr, as a result of which π-allyl c-C_6H_9 dehydrogenates to 1,4-cyclohexadiene.[14] It should be noted that, in the absence of hydrogen, adsorbed benzene is not observed on the Pt(100) surface, while benzene is found on the Pt(111) surface. Another notable difference is that 1,3-cyclohexadiene is never observed on the Pt(100) surface. 1,4-Cylcohexadiene is coadsorbed with π-allyl c-C_6H_9 and cyclohexyl on Pt(100), while cyclohexyl is not found on the Pt(111) surface during the cyclohexene hydrogenation and dehydrogenation reactions.

At low pressures of cyclohexene ($\leq$0.5 Torr) and low surface temperatures, π-allyl c-C_6H_9 is the major surface species on the Pt(100)[24] surface. Increasing pressures to 1.5 Torr of cyclohexene coadsorbs 1,4-cyclohexadiene with π-allyl c-C_6H_9. Further increasing the pressure to 1.5 Torr led to the hydrogenation of 1,4-cyclohexadiene to π-allyl c-C_6H_9 and coadsorbed cyclohexyl.[24] Low pressures ($\leq$0.1 Torr) of cyclohexene on the Pt(111) surface yield π-allyl c-C_6H_9 as the major surface species. Increasing the pressure to 1.5 Torr results in the conversion of

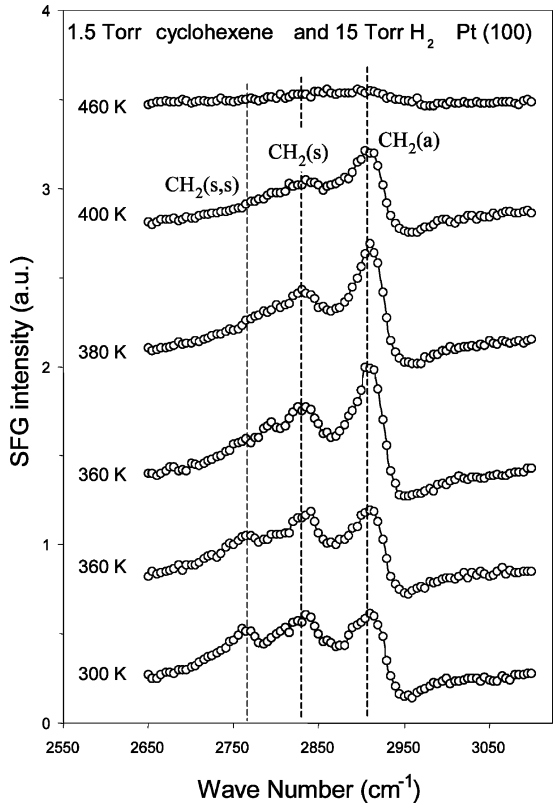

Figure 5. Temperature-dependent SFG spectra of surface species on Pt(100) under 1.5 Torr of cyclohexene and 15 Torr H_2 in the range 300−460 K. Dotted lines were drawn for visual aids.

π-allyl c-C_6H_9 to 1,4-cyclohexadiene at 298 K. Coadsorption of 1,4-cyclohexadiene and π-allyl c-C_6H_9 is not observed on the Pt(111) surface. In the presence of excess hydrogen and under 1.5 Torr of cyclohexene, 1,3-cyclohexadiene is coadsorbed with 1,4-cyclohexadiene. It is important to note that 1,3-cyclohexadiene is not present on the Pt(100) surface under high-pressure conditions; this result may be an influential preference of the dehydrogenation or hydrogenation pathways on the two single-crystal surfaces. Hydrogenation of 1,4-cyclohexadiene to π-allyl c-C_6H_9 on the Pt(111) surface in the presence and absence of excess hydrogen occurs as the surface temperature is increased. Using a bimolecular scheme, the following reaction is proposed.

$$C_6H_8 + C_6H_{10}\ (\text{excess}) \rightarrow 2C_6H_9 \qquad (R3)$$

When the metal surface temperature is increased to 400 K in the presence and absence of excess hydrogen, 1,3-cyclohexadiene appears on the Pt(111) surface. The surface reaction pathways on both Pt(100) and Pt(111) in the absence and presence of H_2 are summarized in Scheme 2.

Kinetic measurements of the dehydrogenation and hydrogenation pathways on Pt(100) in the absence of excess of hydrogen have exhibited similar apparent activation energies: 14.3 ± 1.2 kcal/mol and 12.9 ± 0.6 kcal/mol, respectively.[24] Moreover, on Pt(111) in the same temperature range gave similar apparent activation energies for dehydrogenation/hydrogenation on Pt(111) of 13.5 ± 0.8 kcal/mol and 14.0 ± 0.4 kcal/mol, respectively.[16] These results lend credence to the assumption that in the absence of hydrogen the dehydrogenation and hydrogenation share the same reaction pathway on both the Pt(100) and Pt(111) surfaces. However, dissimilar apparent activation energies (22.4 ± 1.6 kcal/mol for dehydrogenation and 18.8 ± 0.9 kcal/mol for hydrogenation) in the presence of excess hydrogen on Pt(100) imply two distinctive reaction pathways.

Cyclohexane production may be accessed through two different reactions.[17] Stepwise hydrogenation is one of the possible pathways whereby adsorbed cyclohexene reacts with adsorbed hydrogen to form cyclohexyl, and subsequently, cyclohexane evolves (R4). Another pathway is disproportionation or self-hydrogenation (R5), which is normally independent of hydrogen pressure.[17]

$$C_6H_{10} \rightarrow C_6H_6 + 4H \qquad (R4)$$

$$3C_6H_{10} \rightarrow C_6H_6 + 2C_6H_{12} \qquad (R5)$$

The disproportionation reaction is structure-insensitive based on similar apparent activation energies for dehydrogenation and hydrogenation reactions pathways on both the Pt(111)[16] and Pt(100)[24] crystals. However, structure sensitivity exists in the presence of excess hydrogen for the reaction on these surfaces. The reported apparent activation energies of 17.9 ± 0.2 kcal/mol for the dehydrogenation pathway and 8.6 ± 0.1 kcal/mol for the hydrogenation pathway on Pt(111)[16] are quite different than those for the Pt(100)[24] surface.

The surface intermediates responsible for the hydrogenation and dehydrogenation pathways under excess H_2 are not present without H_2, explaining the structure sensitivity of the reaction. Lack of hydrogen adsorbed on the surface may induce this effect. Furthermore, the reactive surface intermediates responsible for the greatly enhanced TORs in the presence of H_2 may hydrogenate rapidly, resulting in similar SFG spectra with and without H_2.

SCHEME 2: Schematic Diagram of Observed Surface Species under 1.5 Torr of Cyclohexene (a) without H_2 on Pt(100), (b) without H_2 on Pt(111), (c) with 15 Torr H_2 on Pt(100), and (d) with 15 Torr H_2 on Pt(111)

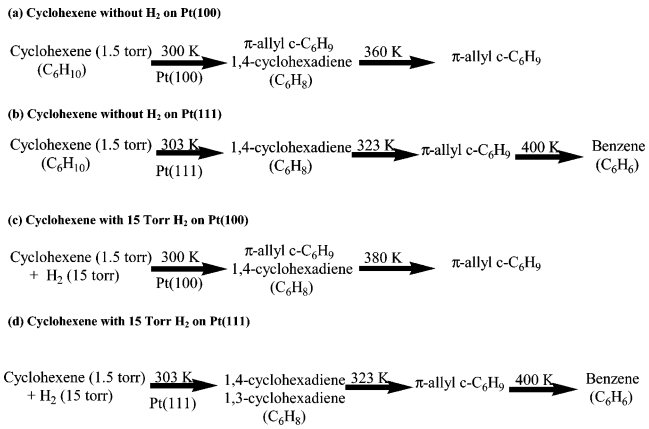

The activation energies measured for catalytic dehydrogenation/hydrogenation on platinum can be understood through the semiempirical thermodynamic analysis of Koel et al.[25] Calculations show that C−H cleavage from π-allyl c-C_6H_9 is a slow step with an activation energy of 22 kcal/mol for adsorbed benzene, which agrees with our results for cyclohexene dehydrogenation on Pt(100). The calculated activation energy of 1,3-cyclohexadiene conversion to benzene is only 7 kcal/mol and has appeared in the sum frequency spectrum on Pt(111). The absence of 1,3-cyclohexadiene on the Pt(100) surface may explain the increased apparent activation energy for dehydrogenation and also confirm that 1.3-cyclohexadiene is an important reactive intermediate in dehydrogenation.

The hydrogenation of the cyclohexyl radical has been calculated to have an activation energy of 17 kcal/mol,[25] which is in agreement with the Pt(100) surface (18.8 ± 0.9 kcal/mol). π-Allyl c-C_6H_9 is found to be adsorbed on the Pt(111) surface via SFG.[14] On Pt(100), π-allyl c-C_6H_9 is coadsorbed with the cyclohexyl C_6H_{11}. The discrepancy in turnovers on Pt(100) and Pt(100) is rationalized by the difference in the SFG spectra on Pt(100) and Pt(111) and implies that different binding sites are favored in the hydrogenation pathway. The activation energy of dehydrogenating to π-allyl c-C_6H_9 is 9 kcal/mol,[25] which agrees with the results on Pt(111) (8.6 ± 0.1 kcal/mol).[14] A hydrogen adatom is left on the surface in the step making it possibly important in the hydrogenation pathway.

III. High-Pressure Scanning Tunneling Microscopy Studies of Cyclohexene Hydrogenation/Dehydrogenation on Platinum Single Crystal (111)

In obtaining a complete understanding of heterogeneous catalysts and their deactivation, learning about surface dynamics on a molecular level is crucial. High-pressure spectroscopic techniques yield information about structure and bonding but lack the spatial resolution necessary to monitor individual adsorbates. High-pressure scanning tunneling microscopy (HPSTM), however, has proven to be an extremely powerful technique for the investigation of catalytic surfaces under reaction conditions. STM has been shown to be able to provide atomically resolved images at elevated pressures and temperatures as long as the surfaces studied are not too mobile. Through studying easily controlled, model catalytic systems with STM, one can elucidate the complex phenomenon of catalysis and gain insight into the most important features of an ideal catalyst. To garner a better understanding of the role of surface

mobility in particular, HPSTM was employed to investigate the hydrogenation/dehydrogenation of cyclohexene on a platinum single crystal and its poisoning with carbon monoxide in the mTorr regime. Concurrently, mass spectrometry was used to monitor whether the catalyst was actively producing gas-phase products. Experiments were performed from 298−353 K.

III.A. Schematic of High-Pressure STM. Measurements using a high-pressure/high-temperature STM system are carried out in equilibrium with the gas phase. The STM portion of the apparatus is a custom-built system from RHK technologies. The STM stage is mounted horizontally on an 8-in flange connected to the rear of the chamber. The chamber can be isolated from the rest of the system by gate valves. This allows introduction of pressures up to slightly above 1 atm into the STM chamber, while the rest of the system remains at UHV. The entire volume of the chamber is approximately 10 L, and it is connected via a 3.5-ft-long $^1/_4$-in-diameter stainless steel tube to a leak valve allowing introduction of low pressures of gas from the STM chamber into the UHV chamber for analysis with the mass spectrometer. The chamber has three additional valves connected to gas cylinders as well as one attached to a liquid sample reservoir.

III.B. Result and Discussions. Upon adsorption to the Pt (111) crystal surface at room temperature (298 K), cyclohexene is known to immediately partially dehydrogenate to form the more stable C_6H_9 π-allyl species (see Scheme 1a).[13,16,25] The low-pressure (1×10^{-6} Torr) structure formed by the π-allyl has been proposed to be a ($\sqrt{7} \times \sqrt{7}$) R19.1°.[26] When the back-pressure of cyclohexene is raised to 20 mTorr, this structure remains intact. If, prior to the introduction of the cyclohexene, the surface is in the presence of 20 mTorr of hydrogen, STM still reveals the same ($\sqrt{7} \times \sqrt{7}$) R19.1° structure formed by π-allyl. A sample image of this surface is shown in Figure 6a. Thus, the presence of background hydrogen at an equal pressure to that of cyclohexene, and thus the saturation of the surface with hydrogen, does not prevent the cyclohexene from dehydrogenating to the more stable π-allyl. The presence of coadsorbed hydrogen also does not weaken the Pt−π-allyl bond sufficiently to cause mobility at room temperature. Analysis of the gas-phase species with mass spectrometry shows no production of either cyclohexane or benzene. Thus, the immobile static surface observed is not catalytically active.

In an attempt to induce a catalytically active surface, the back-pressure of hydrogen was increased to 200 mTorr, while the cyclohexene pressure remained at 20 mTorr. The addition of higher pressures of hydrogen changes the system dramatically. STM images now show a surface with no discernible order as is seen in Figure 6b. Large-scale images (~1000 Å) still reveal the same platinum steps regularly observed, but no molecular surface structure can be resolved in small-scale images (~75 Å). This indicates that the adsorbed monolayer of molecules and atoms is now too mobile to image with the STM. The maximum scanning speed at which images can be obtained is 10 nm/ms, but several scans may be necessary to image an entire molecule. Molecules that diffuse or adsorb/desorb on a faster time scale than this were not able to be resolved. The formation of this mobile overlayer also corresponds to the onset of catalytic activity as monitored by the mass spectrometer. Sustainable production of both cyclohexane, and to a lesser extent benzene, is observed for several hours.

To further understand the catalyst surface, 5 mTorr of carbon monoxide is introduced to intentionally poison the catalyst activity. STM images now show an ordered static overlay of hexagonal symmetry as displayed in Figure 6c. Clearly, all surface diffusion has ceased, as imaging the same area over time yields no changes is surface structure. The structure that is formed appears to be the incommensurate Pt(111) CO structure that has been previously reported[27] and is imaged regularly in our laboratory.[28] All catalytic activity as detected by mass spectrometry has now stopped. Previous studies of ethylene hydrogenation on Pt(111) and Rh(111) in our laboratory suggest that the CO freezes the adsorbed monolayer in place and creates a coadsorbed structure of CO and ethylidyne.[29] This is very unlikely in this case, however, since the larger cyclic C_6 molecules could not be incorporated into the CO structure without drastically changing its periodicity.

These experiments were repeated at 353 K to monitor the effect of temperature on the surface mobility of the poisoned system. Images of the surface in the presence of 200 mTorr of H_2 and 20 mTorr of cyclohexene at 353 K show a completely

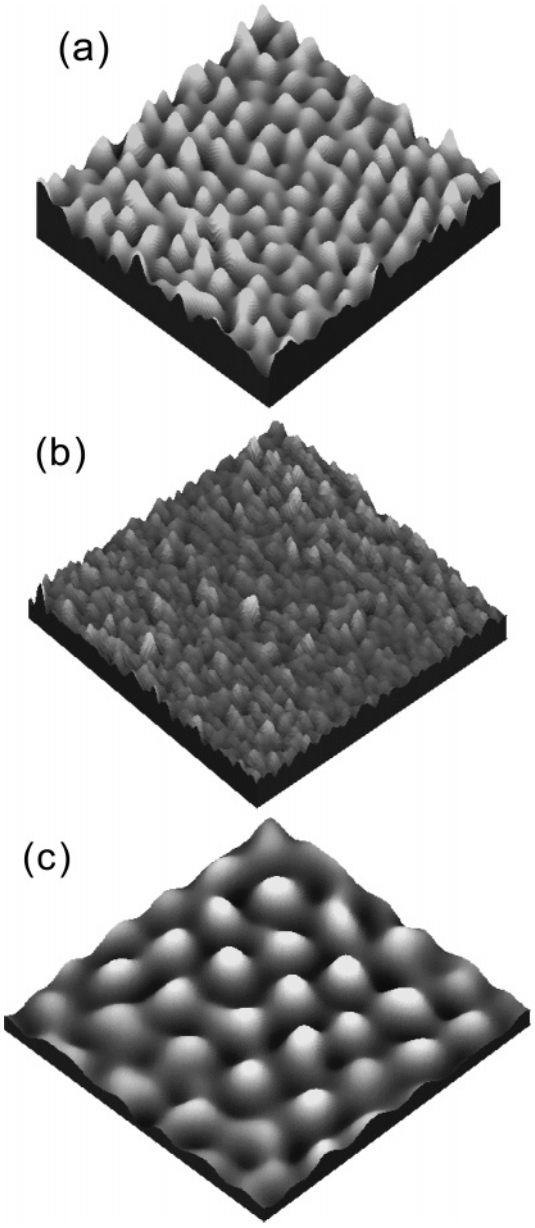

Figure 6. 70 Å × 70 Å STM images of the Pt(111) surface in the presence of (a) 20 mTorr of hydrogen and 20 mTorr of cyclohexene. Surface is catalytically inactive. (b) 200 mTorr of hydrogen and 20 mTorr of cyclohexene. Surface is catalytically active, producing both cyclohexane and benzene. (c) 200 mTorr of hydrogen, 20 mTorr of cyclohexene, and 5 mTorr of CO. Surface has been deactivated.

disordered surface, very similar to those observed at room temperature. Gas-phase cyclohexane and benzene are steadily produced at a faster rate than at room temperature. The rate of benzene production is now higher than the rate of cyclohexane production, though. This phenomenon has been previously reported[9,30] and is not surprising. Introduction of CO into the system resulted in total deactivation of the catalyst, and no products were observed over the course of several hours, yet STM revealed a surface that was still too mobile to image. Other studies of Pt(111)-catalyzed H_2/D_2 exchange under identical conditions did show turnover.[31] High-pressure photoelectron spectroscopy (HPXPS) studies also indicate that only about 10% of the CO present at 298 K is removed by heating to 353 K with a back-pressure of 5 mTorr. We thus propose that the surface is dominated by a mobile CO overlayer containing vacancy aggregates large enough to facilitate H_2 and D_2 adsorption but not large enough for cyclohexene adsorption.

The results of these studies have led us to a few conclusions. Primarily, mobility of a catalytic surface is absolutely necessary for an active catalyst. To date, no catalytically active surface studied in our laboratory has been composed of a static overlayer. This mobility allows for interactions of reactants, as well as freeing up of adsorption sites occupied by poison molecules. If the concentration of poison molecules is too high, however, adsorption may be blocked altogether and reactant molecules may simply not be able to reach the surface. In addition, the coverage of a poison molecule can dictate the likelihood of a gas molecule adsorbing based on the size of the vacancy aggregate necessary for adsorption.

IV. Catalytic Nanodiode

The mechanisms of chemical energy conversion during catalytic reactions are among the important issues of surface science. Exothermic chemical reactions at the surface can dissipate chemical energy by electronic excitation, leading to generation of energetic charge carriers. These energetic charge carriers are often called "hot" or "ballistic" charge carriers.[32,33] When heat is deposited as a result of exothermic surface reactions or photon flux, the electrons heat up much faster (femtoseconds) than the lattice (picoseconds) because of their much lower heat capacity. If the metal particle or film is of the diameter or thickness of the electron mean free path (~10 nm), the electrons can be collected as they are transported across the metal without collision or emission at the metal surface.[34] If the kinetic energy of these energetic electrons is greater than the effective height of the Schottky barrier formed at the metal−semiconductor interface, electrons will move to the semiconductor, leading to the hot electron current. The transport process of hot electrons through a metal−semiconductor contact is illustrated in the energy diagram of Figure 7a. For an n-type Schottky diode, hot electrons are detected as a chemicurrent if their excess energy $E_{ex} = |E - E_F|$ is larger than the effective Schottky barrier, which is the difference between the conduction band minimum and the Fermi energy E_F at the interface.

IV.A. Fabrication of Pt/TiO_2 Catalytic Nanodiode. The platinum catalyst was one of the electrodes of the Schottky nanodiodes fabricated with TiO_2 semiconductors. Figure 7b shows a photograph of a Pt/TiO_2 nanodiode we fabricated. The bottom electrode, including a 50-nm Cr or Ti and a 150-nm Au layer, was first deposited through the first mask onto an oxidized p-type Si(100) wafer under 1×10^{-6} Torr pressure by an electron beam evaporator. The thin films of Cr or Ti improve the adhesion property between the gold layer and the SiO_2. Then, 50 nm of Ti, 2.5 mm × 2.5 mm, was deposited on the top of the bottom electrode to form the Ohmic contact between the bottom electrode and the TiO_2 film. Next, a 150-nm TiO_2 film of 4 mm × 4 mm was deposited by sputtering through a third mask. Since no oxygen was added during the evaporation, a nonstoichometric TiO_x ($x < 2$) film was formed with oxygen vacancies, which increased the free carrier concentration. A strip of 150-nm-thick silicon nitride was then deposited through a fourth mask by plasma-enhanced chemical vapor deposition (PECVD) at room temperature. This layer had high resistivity and was utilized to prevent leakage between the top electrode and the TiO_2 film. Platinum of 2 mm in diameter with a thickness between 1 and 15 nm was then e-beam evaporated through a fifth mask onto the TiO_2. Finally, the front gold electrode was e-beam deposited through the sixth mask onto the silicon nitride and the platinum to complete the diode circuit. For the chemical reaction experiment, a batch reaction system of about 1-L volume was built to carry out the gas-phase reaction. Details on the chemical reactor are described elsewhere.[35]

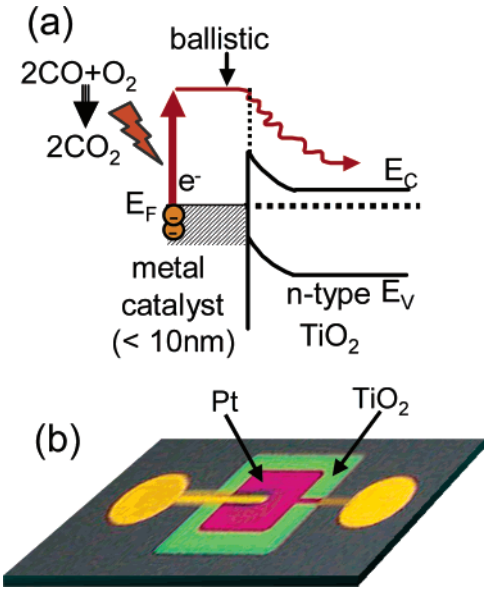

Figure 7. (a) Scheme of the detection of ballistic charge carrier in the catalytic metal−semiconductor Schottky diode. (b) Photograph of Pt/TiO_2 catalytic nanodiode.

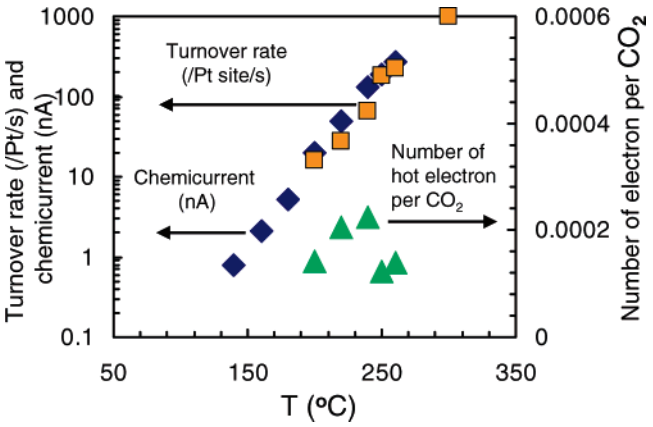

Figure 8. Plot of chemicurrent and turnover rate as a function of the temperature. The number of electrons per CO_2 ($1-2 \times 10^{-4}$) were obtained from the measurement of turnover rate and chemicurrent.

IV.B. Results and Discussions. Production and accumulation of CO_2 molecules were also measured during carbon monoxide oxidation by using gas chromatography. Figure 8 shows the chemicurrent and turnover rate under 100 Torr of oxygen and

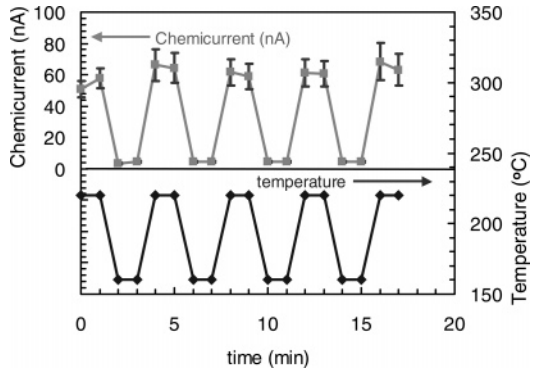

Figure 9. Chemicurrent detected Pt/TiO_2 catalytic nanodiode as changing the sample temperature. The chemicurrent shows the clear reversibility, suggesting the possible application of chemical sensors.

40 Torr of carbon monoxide as a function of the temperature. While the detection of current flow between 140−200 °C is clear, the accumulation of CO_2 in that temperature range is too low to be detected by gas chromatography. This suggests that the hot electron current is a more sensitive probe than gas chromatography to measure and monitor the catalytic chemical reaction. This increased sensitivity of hot electron detection may have potential applications for chemical sensors. The number of electrons per molecules of CO_2 produced is estimated to be $1-2 \times 10^{-4}$ from the measurement of current and turnover rates as shown in the secondary *y* axis. We note that this value depends on the surface cleanliness, the thickness of Pt, and the conductivity of the TiO_2 layer.[36]

From the slope of the Arrhenius plot of chemicurrent and turnover rate in the temperature range 140−300 °C, the activation energy of the carbon monoxide reaction on the Pt/TiO_2 nanodiode is determined. The activation energy obtained from the current measurement is 21 kcal/mol, and a similar value is derived from gas chromatography (22 kcal/mol).[36] This excellent correlation between hot electron flux and turnover rate suggests that the current measurement can indeed be used for monitoring the chemical reaction in a quantitative manner.

For the application of chemical sensors or energy conversion devices, the stability and reversibility of the chemicurrent are quite crucial issues. We monitored the reversibility of chemicurrent by changing the sample temperature. Figure 9 shows the plot of chemicurrent vs time while changing the temperature from 160 °C to 220 °C. The chemicurrent changes reversibly with changing temperature, revealing the clear reversibility of the catalytic nanodiode.

Recently, our laboratory has developed working experience with platinum or rhodium nanowires on different oxide (Al_2O_3, SiO_2, CeO_2, ZrO_2, and Nb_2O_5)[37] films using nanoimprint and size reduction lithography techniques. These metal nanowire−oxide systems allow us to vary the metal−oxide area and the materials in a controllable manner. Also, nanowires on oxides are energetically more stable than thin-film nanodiode, since the platinum film deposited on an oxide surface is likely to be chemically and thermally unstable and to break up into smaller islands upon heating. Lithography techniques would permit us to make electrical contacts to these nanowires on the oxide surface and would allow us to measure the hot electron transport in these well-defined metal−oxide nanostructures. This new scheme of nanowire metal−semiconductor Schottky diode might give insight into the role of hot electron transport in metal−oxide catalysis.

V. Conclusion

The role of surface defects, surface diffusion, and hot electron in dynamics of surface catalyzed reactions are studied with sum frequency generation (SFG), scanning tunneling microscopy (HPSTM), and catalytic nanodiodes. Kinetic measurements and SFG vibrational spectroscopy have allowed us to clarify the reaction pathways during 1.5 Torr of cyclohexene hydrogenation/dehydrogenation in the presence and absence of H_2 at various temperatures on Pt(100) and Pt(111). The rate-determining step for cyclohexene hydrogenation was found to be π-allyl $c\text{-}C_6H_9$ for both surfaces. The dehydrogenation pathway's rate-determining step, however, was determined to be 1,3-cyclohexadiene on the Pt(111) surface and could not be identified on the Pt(100) surface. Hot electron flow through catalytic nanodiodes provides new insights into the role of electronic excitation leading to new energy conversion processes using heterogeneous metal catalysis. We found that the hot electron flux is well-correlated with the turnover rates and selectivity of catalyzed reactions. This also brings us closer to the possibility that hot charge carriers influence the catalytic turnover rate and selectivity.

Acknowledgment. This work was supported by the Director, Office of Science, Office of Basic Energy Sciences, Division of Materials Sciences and Engineering of the U.S. Department of Energy under contract no. DE-AC02-05CH11231.

References and Notes

(1) Ge, N. H.; Wong, C. M.; Lingle, R. L.; McNeill, J. D.; Gaffney, K. J.; Harris, C. B. *Science* **1998**, *279*, 202. Miller, A. D.; Bezel, I.; Gaffney, K. J.; Garrett-Roe, S.; Liu, S. H.; Szymanski, P.; Harris, C. B. *Science* **2002**, *297*, 1163. Lingle, R. L.; Padowitz, D. F.; Jordan, R. E.; McNeill, J. D.; Harris, C. B. *Phys. Rev. Lett.* **1994**, *72*, 2243.

(2) Hagstrom, S.; Lyon, H. B.; Somorjai, G. A. *Phys. Rev. Lett.* **1965**, *15*, 491.

(3) West, L. A.; Somorjai, G. A. *J. Chem. Phys.* **1972**, *57*, 5143.

(4) Kahn, D. R.; Petersen, E. E.; Somorjai, G. A. *J. Catal.* **1974**, *34*, 294.

(5) Cremer, P. S.; Stanners, C.; Niemantsverdriet, J. M.; Shen, Y. R.; Somorjai, G. A. *Surf. Sci.* **1995**, *328*, 111.

(6) Jensen, J. A.; Rider, K. B.; Chen, Y.; Salmeron, M.; Somorjai, G. A. *J. Vac. Sci. Technol.* **1999**, *17*, 1080.

(7) Ji, X. Z.; Zuppero, A.; Gidwani, J. M.; Somorjai, G. A. *Nano Lett.* **2005**, *5*, 753. Ji, X. Z.; Zuppero, A.; Gidwani, J. M.; Somorjai, G. A. *J. Am. Chem. Soc.* **2005**, *127*, 5792.

(8) Antos, G. J.; Aitani, A. M.; Parera, J. M. *Catalyic naphtha reforming: science and technology*, 2nd ed.; Marcel Dekker: New York, 1995.

(9) McCrea, K. R.; Somorjai, G. A. *J. Mol. Catal., A* **2000**, *163*, 43.

(10) Lamont, C. L. A.; Borbach, M.; Marin, R.; Gardner, P.; Jones, T. S.; Conrad, H.; Bradshaw, A. M. *Surf. Sci.* **1997**, *374*, 215.

(11) Pettiette-Hall, C. L.; Land, D. P.; McIver, R. T.; Hemminger, J. C. *J. Am. Chem. Soc.* **1991**, *113*, 2755.

(12) Rodriguez, J. A.; Campbell, C. T. *J. Catal.* **1989**, *115*, 500.

(13) Henn, F. C.; Diaz, A. L.; Bussel, M. E.; Huggenschmidt, M. B.; Domagala, M. E.; Campbell, C. T. *J. Phys. Chem.* **1992**, *96*, 5965.

(14) Yang, M.; Chou, K. C.; Somorjai, G. A. *J. Phys. Chem. B* **2003**, *107*, 5267.

(15) Yang, M.; Somorjai, G. A. *J. Am. Chem. Soc.* **2003**, *125*, 11131.

(16) Yang, M.; Chou, K. C.; Somorjai, G. A. *J. Phys. Chem. B* **2004**, *108*, 14766.

(17) Yang, M.; Dunietz, B.; Head-Gordon, M.; Somorjai, G. A. In publication, 2006.

(18) Su, X.; Shen, Y. R.; Somorjai, G. A. *Chem. Phys. Lett.* **1997**, *280*, 302.

(19) Su, X.; Kung, K.; Lahtinen, J.; Shen, R. Y.; Somorjai, G. A. *J. Mol. Catal., A* **1999**, *141*, 9−19.

(20) Manner, W. L.; Girolami, G. S.; Nuzzo, R. G. *J. Phys. Chem. B* **1998**, *102*, 10295.

(21) Shen, Y. R. *Nature (London)* **1989**, *337*, 519.

(22) Shen, Y. R. *Annu. Rev. Phys. Chem.* **1989**, *40*, 327.

(23) Shen, Y. R. *The Principles of Nonlinear Optics*; Wiley: New York, 2003.

(24) Bratlie, K. M.; Flores, L. D.; Somorjai, G. A. *Surf. Sci.* **2005**, *599*, 93.

(25) Koel, B. E.; Blank, D. A.; Carter, E. A. *J. Mol. Catal., A* **1998**, *131*, 39−53.

(26) Montano, M.; Salmeron, M.; Somorjai, G. A. *Surf. Sci.* **2006**, *600*, 1809.

(27) Longwitz, S. R.; Schnadt, J.; Kruse Vestergaard, E.; Vang, R. T.; Laesgsaard, E.; Stensgaard, I.; Brune, H.; Besenbacher, F. *J. Phys. Chem. B* **2004**, *108*, 14497.

(28) Montano, M.; Tang, D. C.; Somorjai, G. A. *Catal. Lett.* **2006**, *107*, 131.

(29) Tang, D. C.; Hwang, K. S.; Salmeron, M.; Somorjai, G. A. *J. Phys. Chem. B* **2004**, *108*, 13300.

(30) Su, X.; Kung, K.; Lahtinen, J.; Shen, R. Y.; Somorjai, G. A. *Catal. Lett.* **1998**, *54*, 9.

(31) Montano, M.; Bratlie, K.; Salmeron, M.; Somorjai, G. A. Submitted for publication.

(32) Hellberg, L.; Stromquist, J.; Kasemo, B.; Lundqvist, B. I. *Phys. Rev. Lett.* **1995**, *74*, 4742.

(33) Huang, Y. H.; Rettner, C. T.; Auerbach, D. J.; Wodtke, A. M. *Science* **2000**, *290*, 111.

(34) Nienhaus, H.; Bergh, H. S.; Gergen, B.; Majumdar, A.; Weinberg, W. H.; McFarland, E. W. *Phys. Rev. Lett.* **1999**, *82*, 446.

(35) Ji, X. Z.; Somorjai, G. A. *J. Phys. Chem. B* **2005**, *109*, 22530.

(36) Park, J. Y.; Somorjai, G. A. *ChemPhysChem* **2006**, *7*, 1409.

(37) Yan, X. M.; Kwon, S.; Contreras, A. M.; Koebel, M. M.; Bokor, J.; Somorjai, G. A. *Catal. Lett.* **2005**, 105, 127. Yan, X. M.; Kwon, S.; Contreras, A. M.; Bokor, J.; Somorjai, G. A. *Nano Lett.* **2005**, *5*, 745.